Enhanced pyroptosis induction with pore-forming gene delivery for osteosarcoma microenvironment reshaping

Jing-Jun Nie [a,1], Bowen Zhang [a,b,1], Peng Luo [a,1], Maoguo Luo [c], Yuwen Luo [a], Jingjing Cao [a], Honggang Wang [a], Jianping Mao [d], Yonggang Xing [d], Weifeng Liu [e], Yuning Cheng [a], Renxian Wang [a], Yajun Liu [d,**], Xinbao Wu [f], Xieyuan Jiang [f], Xiaoguang Cheng [b,***], Chi Zhang [g], Da-Fu Chen [a,*]

[a] Laboratory of Bone Tissue Engineering, Beijing Laboratory of Biomedical Materials, National Center for Orthopaedics, Beijing Research Institute of Traumatology and Orthopaedics, Beijing Jishuitan Hospital, Capital Medical University, Beijing, China
[b] Department of Radiology, National Center for Orthopaedics, The Fourth Clinical Medical College of Peking University, Beijing Jishuitan Hospital, Beijing, China
[c] Biological & Medical Engineering Core Facilities, School of Life Science, Beijing Institute of Technology, Beijing, China
[d] Department of Spine Surgery, National Center for Orthopaedics, Beijing Jishuitan Hospital, Capital Medical University, Beijing, China
[e] Department of Orthopaedic Oncology Surgery, National Center for Orthopaedics, Beijing Jishuitan Hospital, Capital Medical University, Beijing, China
[f] Department of Orthopedic Trauma, National Center for Orthopaedics, Beijing Jishuitan Hospital, Capital Medical University, Beijing, China
[g] Department of Orthopedics, Peking University International Hospital, Beijing, China

A R T I C L E   I N F O

A B S T R A C T

Osteosarcoma is the most common malignant bone tumor without efficient management for improving 5-year event-free survival. Immunotherapy is also limited due to its highly immunosuppressive tumor microenvironment (TME). Pore-forming gasdermins (GSDMs)-mediated pyroptosis has gained increasing concern in reshaping TME, however, the expressions and relationships of GSDMs with osteosarcoma remain unclear. Herein, gasdermin E (GSDME) expression is found to be positively correlated with the prognosis and immune infiltration of osteosarcoma patients, and low GSDME expression was observed. A vector termed as LPAD contains abundant hydroxyl groups for hydrating layer formation was then prepared to deliver the GSDME gene to upregulate protein expression in osteosarcoma for efficient TME reshaping via enhanced pyroptosis induction. Atomistic molecular dynamics simulations analysis proved that the hydroxyl groups increased LPAD hydration abilities by enhancing coulombic interaction. The upregulated GSDME expression together with cleaved caspase-3 provided impressive pyroptosis induction. The pyroptosis further initiated proinflammatory cytokines release, increased immune cell infiltration, activated adaptive immune responses and create a favorable immunogenic hot TME. The study not only confirms the role of GSDME in the immune infiltration and prognosis of osteosarcoma, but also provides a promising strategy for the inhibition of osteosarcoma by pore-forming GSDME gene delivery induced enhanced pyroptosis to reshape the TME of osteosarcoma.

1. Introduction

Osteosarcoma is the most common malignant bone tumor with a poor prognosis especially in children and adolescents [1,2]. The average 5-year event-free survival of patients under current standard managements has notimproved significantly in the last few decades [2]. Immunotherapy, especially immune checkpoint blocking (ICB) therapy, has achieved certain therapeutic effects in melanoma, head and neck squamous cell carcinoma and non-small cell lung cancer [3]. But osteosarcoma responds little to ICB according to recent clinical reports,

which may be attributed to its low degree of immune cell infiltration [4–6]. Reshaping the TME for effective immunotherapy attracted widespread attention [2,6–8]. Studies proved that tumor cells go through immunogenic cell death (ICD) would release damage-associated molecular patterns (DAMPs), promote tumor-infiltrating immune cells, reshape TME and stimulate adaptive immune response [9–13].

Pyroptosis is a form of ICD triggered by the proteolytic cleavage of GSDMs proteins [14–18]. Upon cleavage by specific caspases and other proteases, the freed N terminal of GSDMs (GSDMs-N) fragments assemble into oligomers and translocate to the plasma membrane to form pores in the cell membrane, which induce the release of DAMPs and proinflammatory cytokines [15]. Recent studies generally focus on inducing pyroptosis by taking advantage of originally expressed GSDMs in tumor cells with chemical [19–22], photothermal [23–25] or photodynamic strategies [26–28]. However, the GSDMs were reported to be inhibited in many tumors, which leads to limited pyroptosis inducing efficacy [14,15]. Moreover, the expression and prognosis of GSDMs and their relationships with immune infiltration in osteosarcoma remain unclear. Therefore, confirming the critical member of GSDMs in regulating the TME of osteosarcoma, as well as their levels, is of significant importance for gene intervention-based osteosarcoma therapy.

Therapy with gene regulation needs powerful carriers to protect functional nucleic acids from degradation and clearance, as well as deliver them into target cells [29,30]. Polyethyleneimine (PEI) is a widely utilized polycation vector [31–34], however, its high density of positive charge may lead to non-specifically binding to serum substances in circulation and decrease gene delivery efficiency [35]. Polyethylene glycol (PEG) can form a hydrating layer to avoid non-specifically binding but also decreases cellular uptake [36,37]. Ethanolamine (EA)-modified poly (glycidyl methacrylate) (PGEA) with abundant hydroxyl groups provided chances for the preparation of polycation-based organic or organic/inorganic carriers with the advantages of PEI and PEG due to their tunable hydroxyl and amnio groups [38–41]. The hydroxyl groups provided the vector with hydration ability as ethylene

glycol units in typical PEGylation nanoparticles, which hinders surface protein adsorption in the delivery system and further decreases the system clearance by the mononuclear phagocyte system [37,39,41]. Thus, the PGEA based gene vector may be of great usefulness in regulating GSDMs levels in osteosarcoma to achieve significant pyroptosis for TME reshaping.

Herein, we first investigated the key members of GSDMs in osteosarcoma based on bioinformatics analysis, and GSDME is found to be closely associated with the prognosis and immune infiltration of osteosarcoma patients. Multiplex immunohistochemical, quantitative real-time PCR (qRT-PCR), and immunochemical staining further confirmed the potential of GSDME as a target for effective osteosarcoma immunotherapy. Then, the pore-forming GSDME gene delivery system (LPAD/GSDME) combined with cisplatin (CDDP) was proposed to induce enhanced pyroptosis and initiate TME reshaping of osteosarcoma (Fig. 1). The polycation vector termed as LPAD was prepared by a ring-opening reaction of EA and ethylenediamine (ED) with poly (glycidyl methacrylate) and atomistic molecular dynamics simulations were performed to evaluate its hydration ability. Functional nucleic acid encoding pore-forming protein GSDME was constructed and loaded into LPAD vectors to obtain the LPAD/GSDME gene delivery system. The LPAD/GSDME complexes were delivered into osteosarcoma tumor cells for upregulation of GSDME expression, combined with the administration of CDDP to further stimulate a high proportion of tumor cell pyroptosis. The pyroptosis initiated the release of proinflammatory cytokines, activated immune cells within TME, recruited more immune cells, activated adaptive immune responses, and created a favorable immunogenic hot TME. The study not only confirms the role of GSDME in the immune infiltration and prognosis of osteosarcoma, but also provides a potential strategy for the pyroptosis-mediated inhibition of osteosarcoma by pore-forming gasdermin gene delivery.
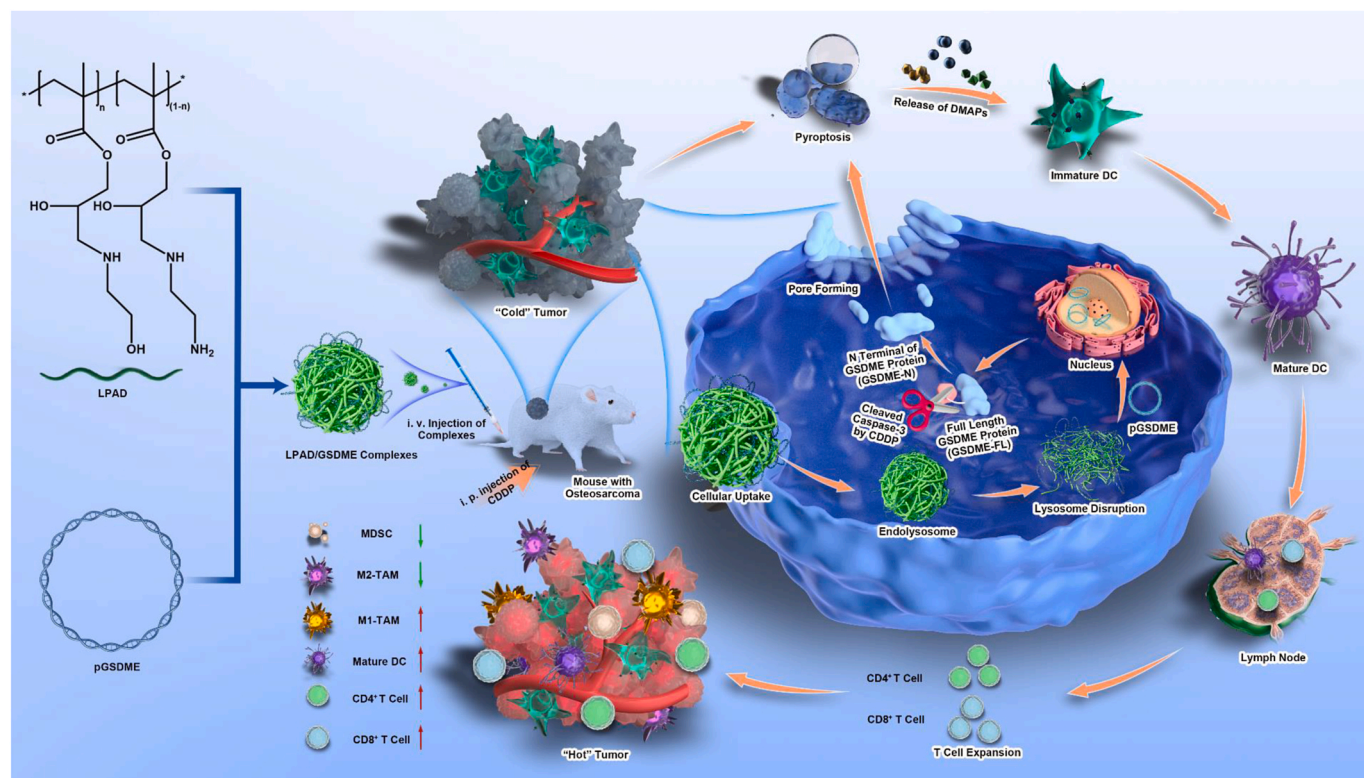
Fig. 1. Illustration of enhanced pyroptosis induction with pore-forming gene delivery for osteosarcoma microenvironment reshaping. Administrations of LPAD/GSDME and CDDP triggers pyroptosis for turning "cold" osteosarcoma into "hot" and eliciting antitumor immunity.

2. Materials and methods

2.1. Materials

Branched polyethyleneimine (PEI, Mw ~25 kDa), N,N,N′,N″,N″-pentamethyldiethylenetriamine (PMDETA, 99 %), ethanolamine (EA, 98 %), ED, and copper(I) bromide (CuBr, 99 %) were purchased from Sigma-Aldrich Chemical Co. (St. Louis, MO, USA). Glycidyl methacrylate (GMA, 98 %), anhydrous dimethyl sulfoxide (DMSO), ethyl 2-bromoisobutyrate (EBA, 98.0 %), and deuterium oxide (D_2O, 99 %) were purchased from Tokyo Chemical Industry Co., Ltd. (TCI, Tokyo, Japan), cell counting kit-8 (CCK8) was purchased from Dojindo (Tokyo, Japan). GelRed™ and Calcein-AM/PI Live/Dead cell double staining kit were purchansed from Beijing Solarbio Science & Technology Co., Ltd. (Beijing, China). Empty plasmid (pDNA), plasmid encoding enhanced green fluorescent protein (pEGFP), plasmid encoding GSDME protein were ordered in GenePharma Co., Ltd. (Shanghai, China). Information about antibodies used in this study was shown in Supplementary Tables 2 and 3

2.2. Molecular dynamics simulation for hydration ability evaluation

Atomistic molecular dynamics simulations were performed to evaluate hydration abilities of LPAD and PEI in aqueous solutions. A repeating unit of LPAD and units of PEI with similarly molecule weights were applied for simulation calculation. The force field parameters of the two polycations were obtained from the Automated Topology Builder and Repository (ATB) version 3.0 [42]. Water molecules were employed by the SPC/E (extended simple point charge) model. Then the simulations were performed with a 2 fs time step in the isothermal-isobaric (NPT) ensemble using the program GROMACS2018. The temperature was fixed at 300 K by using a Nose-Hoover thermostat with a coupling constant of 1.0 ps, and the pressure was controlled at 1 bar with a coupling constant of 2 ps by a semiisotropic Parrinello Rahman barostat. The covalent bonds were constrained using the Lincs algorithm. The Lennard-Jones parameters for the nonbonded interaction between LPAD with water or PEI with water were determined with the conventional Lorentz-Bertelot combining rules. Electrostatic interactions were computed using the Particle-Mesh-Ewald algorithm, and a cutoff of 12 Å was used for the Coulombic and Lennard-Jones interactions. To ensure the overall charge neutrality of the simulated system, appropriate amounts of sodium ions were added by replacing water molecules. A periodic boundary condition was applied along three directions. The units of LPAD and PEI were constructed using packmol package and balanced for 500 ns prior the simulating interaction calculation with water molecules.

2.3. Osteosarcoma patient specimens

Osteosarcoma tissues punctured from patients were obtained and histologically confirmed by Beijing Jishuitan Hospital. This study was approved by the ethics committee of Beijing Jishuitan Hospital (202002–07). And the multiplex immunohistochemical (mIHC) was performed in tumor tissue to evaluate the immune TME of the clinical samples. The paired adjacent tissues and tumor tissues were also investigated with qRT-PCR.

2.4. Tissue microarray (TMA)

A total of 71 formalin-fixed paraffin-embedded osteosarcoma specimens were placed in the TMA (3 samples were invalid) and the TMA was purchased from Xi'an Bioaitechnology Ltd., Co. The expression of GSDME was detected by immunohistochemical assay (IHC), positive scores were evaluated by digital pathology slide scanner, KFBIO.

2.5. Cell viability assay of osteosarcoma cells with various treatments

Briefly, K7M2 cells were seeded in 96-well plates at a density of 1×10^4 cells per well and cultured for 24 h. The cells in control group were treated with PBS for 4 h, and incubated in fresh medium for additional 26 h; in CDDP group were treated with cisplatin (20 μg/mL) for 6 h after additional 24 h incubation; in LPAD/pDNA group were treated with LPAD/pDNA complexes for 4 h, and incubated in fresh medium for additional 26 h; in CDDP + LPAD/pDNA group were treated with LPAD/pDNA complexes for 4 h, then cisplatin (20 μg/mL) were added and incubated for 6 h after additional 20 h incubation in fresh medium; in LPAD/GSDME group were treated with LPAD/GEDME complexes for 4 h, and incubated in fresh medium for additional 26 h; in CDDP + LPAD/GSDME group were treated with LPAD/GEDME complexes for 4 h, then cisplatin (20 μg/mL) were added and incubated for 6 h after additional 20 h incubation in fresh medium. The corresponding cell viabilities were detected by CCK8 assay.

2.6. Evaluation of pyroptosis in vitro

K7M2 cells were seeded in a 24-well plate at a density of 5×10^4 cells per well and cultured for 24 h. Cells with different treatments were the same as in cell viability detection. Briefly, cells were treated with PBS, LPAD/pDNA complexes or LPAD/GSDME complexes for 4 h. Then, the medium with complexes were replaced by fresh medium and incubated for additional 20 h. In the CDDP, CDDP + LPAD and CDDP + LPAD/GSDME groups, the culture medium was replaced with cisplatin at the concentration of 20 μg/mL and cells were incubated for additional 6 h. After that, to examine the changes in cell morphology, annexin V-FITC and propidium iodide (PI) were added to the cell culture medium. Incubated for 15 min in the dark. Fluorescence microscope was used to capture live cell images for studying changes in cell morphology of pyroptosis. The images were captured in at least three randomly selected fields.

To quantitatively analyze pyroptotic cells, flow cytometry was performed to determine the number of annexin V-FITC and PI-positive cells. All cells collected from each 24-well plate wells were washed twice with binding buffer and stained by using an Annexin V-FITC/PI apoptosis detection kit (Solarbio, China).

The release of LDH was measured with CytoTox 96® Non-Radioactive Cytotoxicity Assay, following the manufacturer's instructions.

2.7. Tumor models establishment

All animal studies were approved by Animal Ethics Committee of the Beijing Jishuitan Hospital. BALB/c female mice aged 4–6 weeks were purchased from the Charles River Laboratory and housed in a temperature-controlled environment on a 12 h light cycle with free access to food and sterile water. All mice were allowed to acclimate for at least 3 days before tumor cell implantation.

For an osteosarcoma bearing mouse model, 1×10^6 K7M2 cells in 50 μL of sterile PBS were implanted subcutaneously into the left back of BALB/c female mice. Tumor volume was measured every two days using a Vernier caliper and calculated as $V = (a \times b^2)/2$, where a is the long axis and b is the short axis of the tumor.

2.8. Accumulation analysis of LPAD gene delivery system and tumor inhibition assay in vivo

To detect LPAD mediated DNA accumulation in osteosarcoma, nine K7M2 osteosarcoma bearing mice were divided into 3 groups including control and LPAD/DNA-Cy5 group. The control group was administrated with 100 μL of PBS, the LPAD/DNA-Cy5 group was administrated with 100 μL of LPAD/DNA-Cy5 complexes at the N/P ratio of 15 (20 μg DNA-Cy5 per mouse) via tail vein injection, and the Cy5 group was

administered with 100 μL of equal number of fluorescent molecules. The accumulation of the LPAD/DNA-Cy5 complexes in mice were detected and photographed by in vivo imaging system (IVIS, Perki-nElmer, USA). Representative tissues were also collected for observation.

For tumor inhibition studies, mice were treated with PBS, CDDP, LPAD/GSDME, and CDDP + LPAD/GSDME one week after tumor inoculation (Fig. 6c). CDDP + LPAD/GSDME group, 100 μL of LPAD/GSDME complexes at the N/P ratio of 15 (20 μg GSDME plasmid per mouse) was administered via tail vein injection on days 1, 3, 8, 10, 15 and 17 for a total of six doses; cisplatin was injected intraperitoneally at a dose of 2 μg/g on days 4, 6, 11, 13, 18 and 20 for a total of six doses. During the study, mice were checked daily for adverse clinical reactions. The body weight of mice was monitored every two days until the end of the experiments. 21 days later, all mice were ethically sacrificed. Heart, liver, spleen, lung, kidney, lymph node, tumor tissues and blood were collected for further investigations. And all collected tumor tissues were weighed and photographed.

In vivo toxicity was also detected with hematoxylin and eosin (H&E) staining in main organs. The plasma biochemical analysis of collected blood samples were also performed to evaluate the biosafety of CDDP + LPAD/GSDME combination therapy.

The tumor tissues were further evaluated by using HE staining, terminal deoxynucleotidyl transferase dUTP nick end labeling (Tunnel) staining and immunohistochemistry assay. CD4$^+$ T cells and CD8$^+$ T cells in tumor tissues were observed with immunofluorescent staining.

2.9. Flow cytometry for immune cells

Antibodies for flow cytometry analysis are listed in Table S3. The expression of stimulatory markers of mDCs (CD11c$^+$CD80$^+$CD86$^+$), helper T cells (Ths) (CD3$^+$CD4$^+$), cytotoxic T lymphocytes (CTLs) (CD3$^+$CD8$^+$), M1-macrophages (CD11b$^+$CD86$^+$), M2-macrophages (CD11b$^+$CD206$^+$) and myeloid-derived suppressor cells (MDSCs) (CD11b$^+$Gr-1$^+$) were analyzed by flow cytometry. Briefly, tumors and lymph nodes were harvested and digested by 1 mg/mL collagenase D (Sigma-Aldrich, USA), 20 μg/mL DNase I (Sigma-Aldrich, USA) and 0.1 mg/mL hyaluronidase (Sigma-Aldrich, USA) for 30 min at 37 °C to obtain single-cell suspensions. The single-cell suspensions were then passed through 70-μm nylon cell strainers. The suspension was centrifuged, and the cell pellets were washed and resuspended in the PBS containing 1 % FBS (FACS buffer), blocked by purified rat anti-mouse CD16/CD32 antibody for 30 min, and finally stained with the indicated antibodies for another 45 min. The stained samples were detected using a FACS analyzer (FACSAria^{TM}III, BD, USA). All flow cytometry data were analyzed using FlowJo software.

2.10. Rechallenge experiment

Osteosarcoma bearing mice with a K7M2 tumor on the left back were firstly established as described above. One week after first tumor cell inoculation, each mouse in CDDP + LPAD/GSDME group was treated with 100 μL of LPAD/GSDME complexes at the N/P ratio of 15 (20 μg GSDME per mouse) on days 1, 3 and 2 μg/g cisplatin on days 4, 6. Mice in control group were treated with PBS (Fig. 8d). 10 days later, Mice in both groups were rechallenged with the inoculating of 2×10^6 K7M2 cells on the right back. After another 20 days, all mice were ethically sacrificed. Osteosarcoma tissues were excised and photographed. Corresponding concatenation analysis was carried out with FlowJo v10.8.1. Firstly, DownSample plugin has been employed to ensure that each sample has the same cell number in the FSC/SSC population—the initial gate for the analysis. Then the FSC/SSC population of each group was concatenated into a new FCS file. Finally, all the positive events in each group shown in a density plot can be figured out after drawing gates.

2.11. Statistical analysis

All results are analyzed using GraphPad Prism 8.0 and R (version 4.2.2), presented as the means ± SD. Paired t-test was applied for comparing the mRNA expression of the specimens of osteosarcoma patients. Cox regression analysis was performed in survival analysis. Finally, all the correlation analysis was analyzed by Pearson's correlation analysis. Unpaired t-test and one-way ANOVA were used for two-group or multiple-group comparisons. The details of statistical analysis for figures and Supplementary Figures are performed as indicated in the figure legends, and survival analysis was analyzed using the log-rank test. In all tests, the statistical significance for the tests was set at *p < 0.05, **p < 0.01 and ***p < 0.001.

3. Results

3.1. GSDME in GSDMs play important role in prognostic of osteosarcoma patients and closely correlates with immune infiltration in TME of osteosarcoma

We firstly explored whether GSDMs expressions were associated the prognosis of patients with osteosarcoma. The RNAseq data and corresponding clinical information of osteosarcoma patients were derived from UCSC XENA and analyzed with R (Fig. 2a). It can be inferred that three gasdermin family members, GSDMA, GSDMB, and GSDME, were closely associated with the overall survival of osteosarcoma patients. Patients with higher expression of GSDMA or GSDME had a longer overall survival time. Besides, GSDMB expression was negatively correlated with overall survival in osteosarcoma.

Then we processed correlation analysis to explore the expression relationship between the genes predicted as GSDMs-associated genes and GSDMs in osteosarcoma (Fig. S1). GO and KEGG analyses were conducted after excluding the irrelevant genes (Fig. 2b). The biological process (BP) results indicated that these genes were primarily involved in positive regulation of cysteine-type endopeptidase activity, interleukin-1 secretion, tumor necrosis factor-mediated signaling pathway, interleukin-18 production, and so on. Cellular component (CC) annotations revealed that these genes function as components of inflammasome complex and always work in the cytosolic part, whereas the main molecular function (MF) is comprised of cysteine-type endopeptidase activity, cysteine-type endopeptidase activator activity and peptidase activator activity involved in apoptotic process. The enriched KEGG pathways primarily included NOD-like receptor signaling pathway, cytosolic DNA-sensing pathway, and necroptosis.

The majority of normal cells in tumor tissue are infiltrating stromal and immune cells, which not only disrupt the tumor molecular signal but also play a critical role in cancer biology [43]. Therefore, we inferred the relationship between the expression levels of GSDMs and the abundance of immune cells and stromal cells in osteosarcoma using ESTIMATE analysis. The expression levels of GSDMA, GSDMC, GSDMD and GSDME in osteosarcoma were negatively correlated with tumor purity, while the expression levels of GSDMA, GSDMD and GSDME were positively linked to the abundance of immune cells and stromal cells in osteosarcoma (Fig. 2c). We also investigated the association of GSDMs expression with 28 types of infiltrating immune cells by performing ssGSEA analysis. As shown in Fig. 2d, GSDMD and GSDME were shown to be favorably correlated with up to 27 different types of immune cells, while GSDMA was discovered to have a beneficial relationship with 26 distinct types of immune cells. Taken the above bioinformatics analysis results together, GSDME in gasdermin family is closely associated with prognosis and immune infiltration in TME of osteosarcoma patients.

3.2. GSDME is a potential target for gene intervention in osteosarcoma therapy

To further confirm the potentials of GSDMs in osteosarcoma therapy,
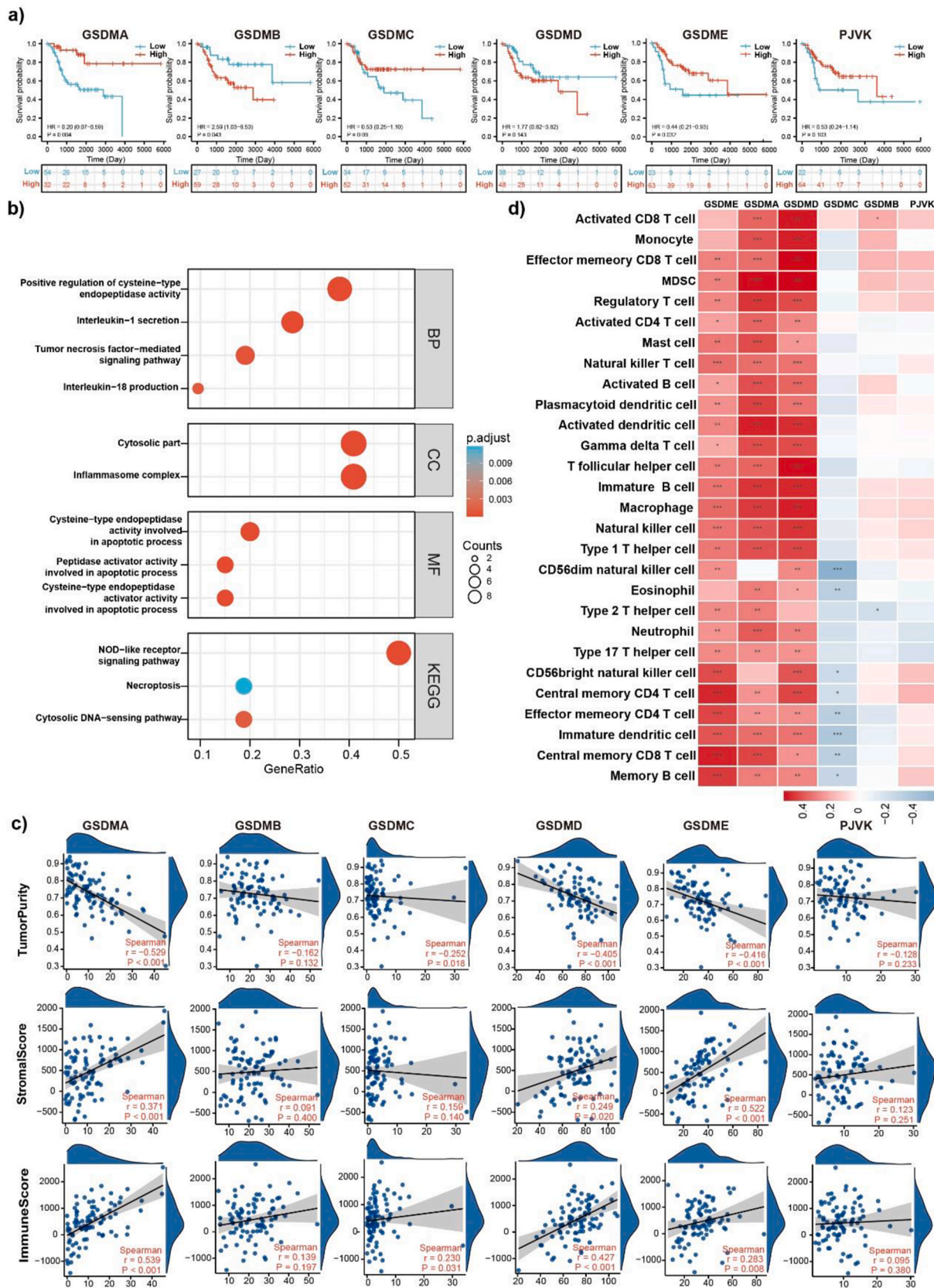
Fig. 2. Gasdermin family is a prognostic biomarker and correlates with immune infiltration in osteosarcoma. a) The Kaplan-Meier survival curves of gasdermin family in osteosarcoma. HR, hazard rate. b) GO and KEGG analyses of GSDMs family-associated genes. GO, Gene Ontology; KEGG, Kyoto Encyclopedia of Genes and Genomes; BP, biological processes; CC, cell component; MF, molecular function. c) the relation of GSDMs expression with the immune score evaluated by ESTIMATE. ESTIMATE, a method that uses gene expression signatures to infer the fraction of stromal and immune cells in tumor samples. d) Relations between the expression of GSDMs and 28 types of tumor-infiltrating lymphocytes in osteosarcoma. (ns, no significance, *$p < 0.05$, **$p < 0.01$, ***$p < 0.001$).

we do further investigations by using clinical samples (Fig. 3). The multiplex immunohistochemical of immune cell infiltration in clinical samples showed low density of tumor-infiltrating-lymphocytes cells (TILs, CD3 positive) and natural killer cells (NK cells, NCR1 positive); and high densities of MDSCs, CD33 positive) and regulatory T cell (Tregs, Foxp3 Positive) (Fig. 3a). The typical results confirmed the immune suppressive TME of osteosarcoma as reported [5,6,44].

GSDMs expressions in osteosarcoma were also evaluated. We firstly applied qRT-PCR in 5 osteosarcoma cell lines (including 143B, Saos-2, U2OS, OS732 and MG63) and their cell-of-origin as bone marrow-derived mesenchymal stem cell (BM-MSC) (Fig. 3b). Remarkably, the mRNA expression levels of GSDMA and GSDME significantly decreased in all osteosarcoma cell lines, which indicated that the expression levels of GSDMA and GSDME were significantly lower in osteosarcoma than in control BM-MSC.

To further verify the above conclusion, we then processed qRT-PCR with 20 pairs of matched osteosarcoma samples and adjacent normal tissues. And the expression differences between tumor tissues and cell lines may be attributed to that there are various types of cells in the tumor tissue, like immune cells, fibrocytes or vascular endothelial cells, thus the gasdermin expressions of tumor tissues is not completely from osteosarcoma cells (Fig. 3c). Interestingly, the GSDME mRNA expression were downregulated in osteosarcoma samples compared to normal tissues (Fig. 3c), which was further investigated in TMA. It can be concluded that the expression of GSDME in patients with early osteosarcoma (IA+IIA, AJCC STAGING SYSTEM) was significantly higher than that in patients with advanced osteosarcoma (IIB+IVB, AJCC STAGING SYSTEM) (Fig. 3d–f), which further indicated that higher expression of GSDME was associated with promising prognosis of patients and confirmed the positive role of GSDME in osteosarcoma therapy.

3.3. Preparation and characterization of LPAD polycation gene vectors

To prepare vectors for pore-forming GSDME functional gene delivery, PGMAs were successfully synthesized by atom transfer radical polymerization (ATRP) with EBA as initiator and GMA as the monomer as reported [44]. Then, EA and ED inducted ring-opening reaction of PGMA polymers were performed and LPAD polycations were synthesized (Fig. 1). ^{1}H NMR was used to confirm the preparation of LPAD polycations and typical spectrum of was shown in Fig. S2. This result proved that PGMA was completely ring-opened and LPAD polycation were prepared successfully.

The capability of nonviral polycations to effectively condense DNA, as well as the size and surface charges of polycation/pDNA complexes are important for cellular endocytosis and biocompatibility. The typical electrophoretic mobilities of the LPAD/pDNA complexes at various N/P ratios in agarose gels (Fig. 4a). It can be concluded that LPAD showed impressive DNA condense ability and prevented the mobility of loaded pDNA at the N/P ratio of 1. The particle sizes of LPAD/pDNA complexes decreased with the increase of N/P ratios at low N/P ratios (N/P ratio≤20), and increased slightly with the continue increase of N/P ratios (Fig. 4b). At low N/P ratios, the condense ability of LPAD was limited due to the low amount of LPAD polycation in LPAD/pDNA complexes and the formed complexes was loose. LPAD amount in the LPAD/pDNA complexes increased with the increase of N/P ratios, which provided increased condense ability and results in the formation of more compact nanoparticles. The slightly increase of particle size at high N/P ratios (N/P = 25) may be attributed to the excess and free LPAD polycations in LPAD/pDNA complexes. Moreover, suitable particle size of the nanocarrier for tumor treatment is necessary which has been reported to be 70–200 nm [39,45]. In other words, the LPAD polycations were potential vectors for gene delivery due to its suitable sizes after condensing DNA (~150–200 nm).

We then observed the surface morphology of the LPAD/pDNA complex at N/P = 15 b y atomic force microscopy (Fig. S3), and the

results showed that most compact complexes existed in the form of relatively uniform spherical nanoparticles. The results proved that LPAD polycations showed great potential in condensing and delivering DNA with suitable sizes and potentials.

The zeta potential of LPAD/pDNA increased with the increase of N/P ratios firstly, and then kept almost constant (Fig. 4b). The changes can be attributed to the increased positive charged LPAD polycation amount in LPAD/pDNA complexes. While the N/P ratios increased continually (N/P = 20 and 25), the introduced LPAD polycations were excess and part of them were free in the solution rather than participated in forming the LPAD/pDNA gene delivery complexes. Thus, the zeta potential almost kept constant.

Additionally, we also prepared LPAD/GSDME complexes at the N/P ratio of 15 to measure its size and surface charge (Fig. S4). We found that the particle size and zeta potential of LPAD/GSDME complex were similar to the LPAD/pDNA complex at 30 min, which confirmed the practicable by using pDNA as demo for the biophysical and chemical characterizations of LPAD polymer. Particle size and zeta potential changes along time were also investigated for stability detection of LPAD/GSDME complexes. As shown in Fig. S4, shows that the particle size of LPAD/GSDME complexes kept almost constant in 8 h, while the particle size of PEI/GSDME increased after 4 h. In other words, LPAD/ GSDME complexes was more stable than PEI/GSDME.

3.4. Hydration ability of LPAD polycation gene vectors determined by molecular dynamics simulation

To further confirm the hydration ability of synthesized LPAD polycation, molecular dynamics simulation was performed to evaluate the nonbonded interaction between polycations and water molecules. As shown in Fig. 4c, synthesized LPAD showed higher total potential energy, which indicated a stronger interaction with water molecules. Further coulombic interaction and Lennard-Jones interaction analysis showed that the hydroxyl groups introduction provided LPAD stronger coulombic interaction with water in comparison with PEI, and results in enhanced total interaction between LPAD and water (Fig. S5). The molecular dynamics simulation proved that LPAD vector showed tight associations with water molecules, which could result in the formation of a hydrating layer. The hydrating layer in turn hinders protein adsorption and subsequent clearance by the mononuclear phagocyte system [37,39]. Non-specific protein absorption assay proved that in comparison with PEI (Fig. 4d), the synthesized LPAD vector showed higher anti-protein absorption ability, which benefited from the stronger hydration ability brought by introduced hydroxyl groups.

3.5. Cytotoxicity and transfection efficiency of LPAD polycation gene vectors

Cytotoxicity is another key factor to evaluate a gene carrier [35,36, 39]. To further evaluate the potentials of LPAD polycations as vectors for gene therapy in osteosarcoma, the cytotoxicity of LPAD polycations at different N/P ratios in various cell lines including HEK293 and K7M2 were analyzed by CCK8 assays and Calcein-AM/PI Live/Dead staining, respectively (Fig. 4e and Fig. S6). The cytotoxicity of all polycation/pDNA complexes increased with the increase of N/P ratios and co-incubation time. In comparison with the PEI/pDNA complexes at the same N/P ratios, cells treated with LPAD/pDNA showed higher cell viability. This can be attributed to the abundant hydroxyl groups in LPAD polycations, which could form a hydration shell to prevent potential cytotoxicity caused by the positive charge (Fig. 4c and d).

Transfection efficiency is also of great importance for gene delivery system. To evaluate the potential of LPAD polycations, pEGFP plasmid encoding enhanced green fluorescent protein was used to show the LPAD polycations mediated cell transfection at different N/P ratios (Fig. 4f). It can be observed that the LPAD vector mediated gene delivery system showed higher positive cell percentages than PEI, especially in
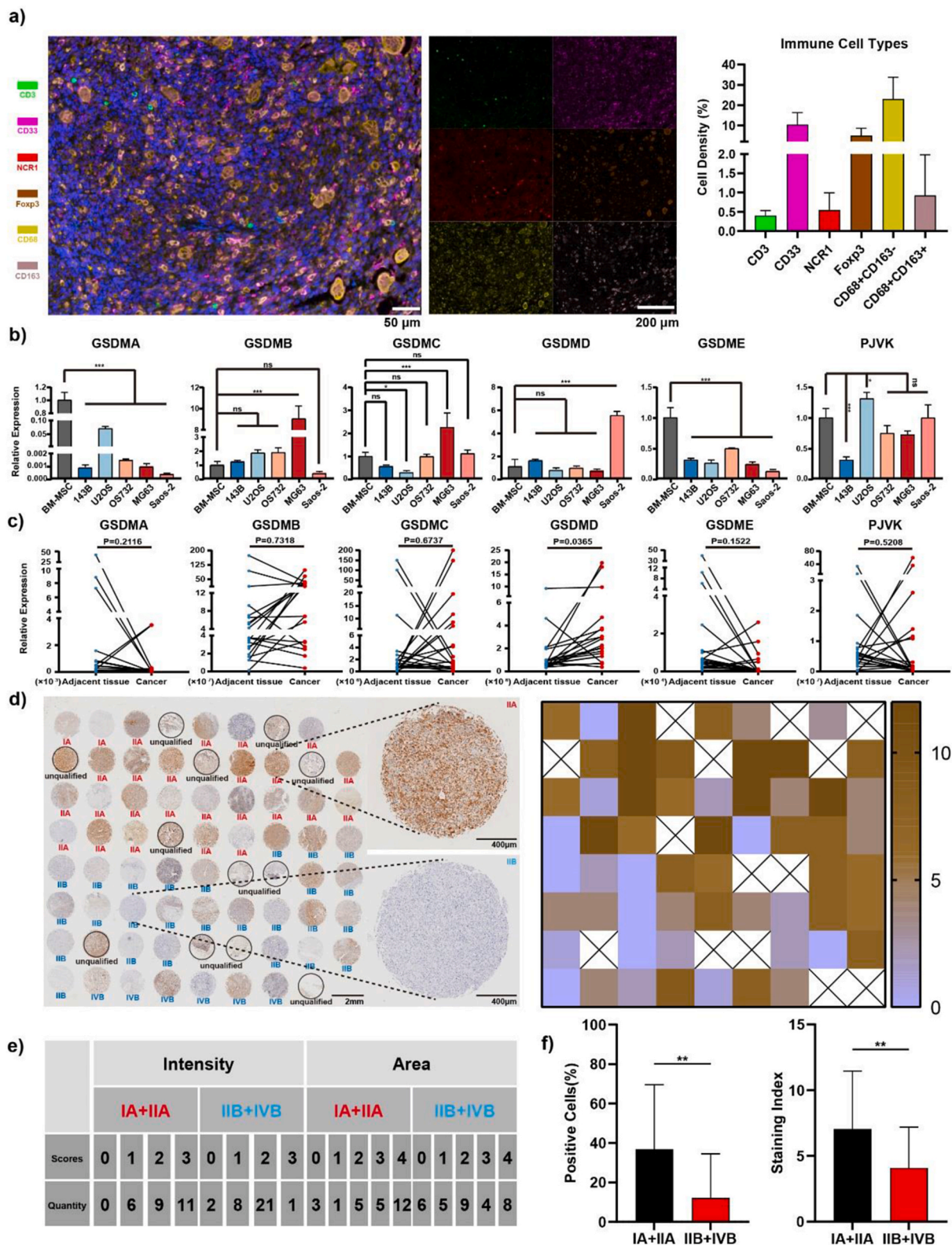
Fig. 3. Characteristics of osteosarcoma microenvironment in clinical samples and the GSDMs expressions. a) The expression of six markers of different tumor-infiltrating lymphocytes. b) The mRNA expression levels of GSDMs family in 5 kinds of osteosarcoma cell lines and its cell-of-origin as BM-MSC. c) GSDMs expressions in 20 osteosarcoma patient specimens and their corresponding adjacent normal tissues. d) the Immunohistochemistry staining of GSDME in osteosarcoma TMA and its corresponding heatmap. Unqualified, the spots in the TMA where osteosarcoma tissues detached from the TMA. e,f) Statistical analysis of differential GSDME expression in TMA of human osteosarcoma tissues. Intensity means expression intensity (score = 0: no expression; score = 1: low expression; score = 2: intermediate expression; score = 3: intensive expression). Area means expression scope (score = 0: positive cells<5 %; score = 1: positive cells is between 6 and 25 %; score = 2: positive cells is between 26 and 50 %; score = 3: positive cells is between 51 and 75 %; score = 4: positive cells>75 %). Staining index = intensity scores × area scores. (ns, no significance, *$p < 0.05$, **$p < 0.01$, ***$p < 0.001$).
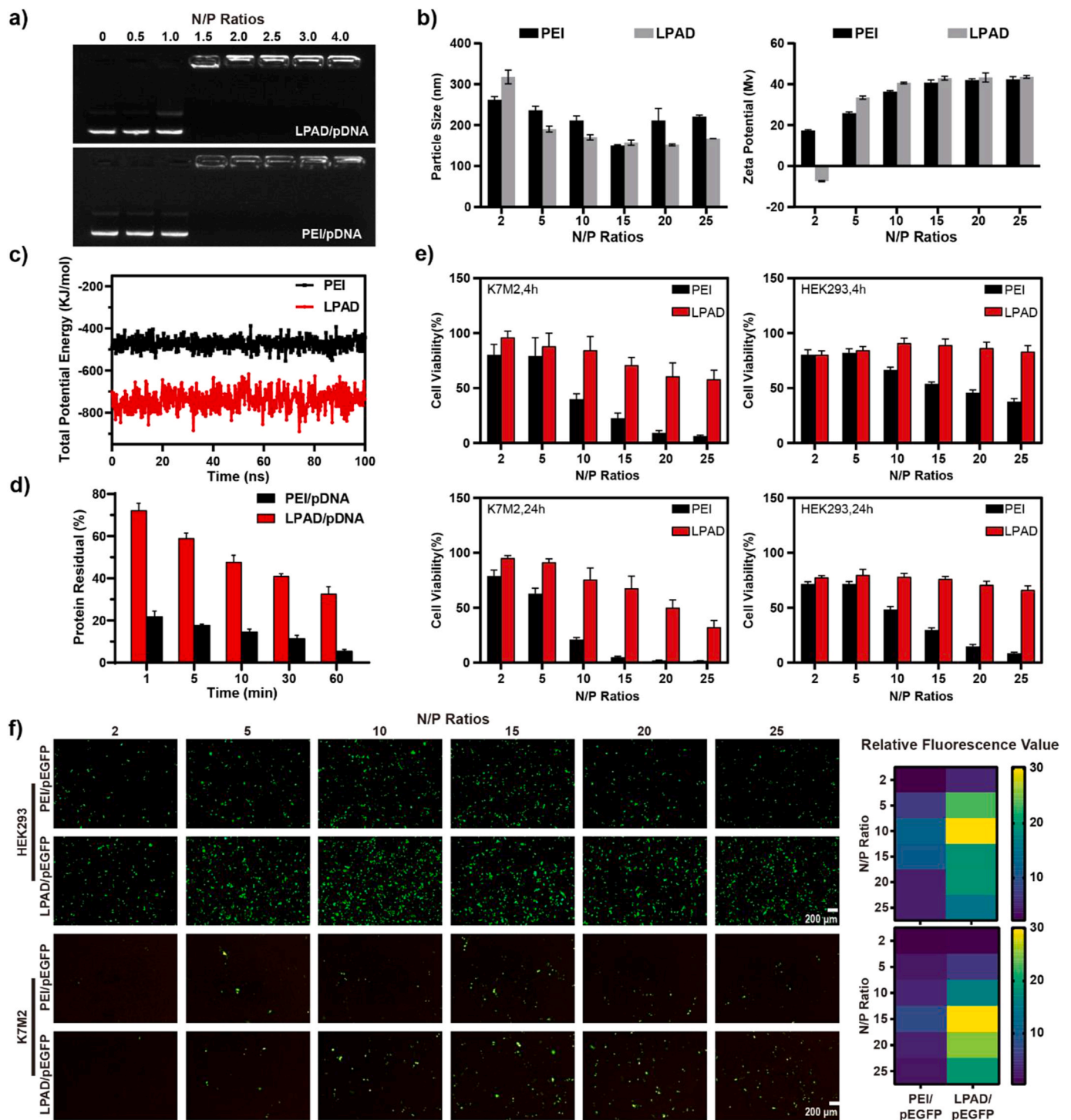
Fig. 4. Biophysical properties of LPAD gene vectors. a) Electrophoretic mobility retardation assays mediated by LPAD for delivering pDNA at various N/P ratios. b) Particle sizes and zeta potentials of LPAD/pDNA complexes. c) Total interaction potential energy plots for LPAD and PEI with water molecules. d) Protein absorption of different polycation-based gene delivery system. e) Cytotoxicity of LPAD in HEK293 and K7M2 cell lines at various N/P ratios. f) Transfection efficiencies of LPAD in HEK293 and K7M2 cell lines evaluated by delivering EGFP plasmid.

high N/P ratios, and the results may be attributed to the better LPAD biocompatibility. The percentages of positive cells increased with the increase of N/P ratios (N/P ≤ 15) which indicated an increase of transfection efficiency. At higher N/P ratios, excess polycations increased cytotoxicity (Fig. 4e and Fig. S6), which making the decrease of transfection efficiency. Thus, the N/P ratio of 15 was supposed as appropriate N/P ratio of LPAD/pDNA complexes and applied in the following experiments.

Cellular uptake in K7M2 cells was performed to confirm the ability of LPAD polycation to deliver nucleic acids. As shown in Fig. S7, LPAD showed higher endocytosis efficiencies than PEI in various N/P ratios, which indicated the stronger gene delivery ability of LPAD and benefited the higher transfection efficacy (Fig. 4f). And the results may be attributed to the larger zeta potentials of LPAD/pDNA complexes (Fig. 4b and Fig. S4).

3.6. LPAD/GSDME gene delivery system combined with CDDP initiate enhanced pyroptosis

The above the bioinformatics analysis results, together with molecular biology and pathology results proved the potential of GSDME intervention in inducing ICD to reshape TME for efficient inhibition of osteosarcoma. The pore-forming gene delivery system LPAD/GSDME was constructed by loading GSDME functional plasmid (encoding pore-forming GEDME protein) into LPAD polycations. Cell viabilities of LPAD/GSDME and PEI/GSDME complexes were detected in BM-MSC cells to further study the safety of LPAD-based delivery system. As shown in Fig. S8, LPAD/GSDME complexes exhibited higher cell viability than PEI/GSDME complexes, which further confirmed the biosafety of LPAD/GSDME gene delivery system.

The LPAD/GSDME system effectively upregulated GSDME protein expression in HEK293 and K7M2 cell lines (Fig. 5a). The antitumor effects of different treatments were also tested in vitro (Fig. 5b). Compared with the control group, the addition of chemotherapeutic CDDP could significantly inhibited the viability of K7M2 cells, for that CDDP could binding to DNA in tumor cells and inhibiting its replication [46]. The viability of osteosarcoma cells in the LPAD/GSDME group was also inhibited. Interestingly, LPAD/GSDME combined with CDDP (CDDP + LPAD/GSDME) can dramatically inhibit osteosarcoma cell viability compared with other groups. It may because that the combination strategy effectively induces pyroptosis, and achieved most significant cell viability inhibiting efficiency.

As shown in Fig. 5c and Fig. S9, pyroptotic morphological changes (pointed with white arrowheads) involving cytoplasmic swelling and membrane rupture were dramatically observed in the CDDP + LPAD/GSDME group (cells treated with LPAD/GSDME combined with CDDP), while these phenomena were hardly observed in other groups. The pyropotosis is directly mediated by assemblies of the GSDMs-N fragments (cleaved production of GSDMs) [16–18]. Flow cytometry was then performed to quantify the pyroptotic cells after different treatments (Fig. 5d and Fig. S10). No surprisingly, LPAD/GSDME combined with CDDP led to dramatically improved pyroptotic cell rates (61.6 %), outperforming other groups by a wide margin. Herein, the two prerequisites for the occurrence of pyroptosis were enough GSDME protein expression and cleavage of GSDME proteins. GSDME protein was over-expressed in osteosarcoma cells by LPAD/GSDME delivery system, meanwhile, chemotherapeutic CDDP was administrated to inducing cleavage of Caspase-3 which further cleaved GSDME protein into *N*-terminal domain and *C*-terminal domain, and the GSDME-N fragments assembled and translocated to cell membrane to induce cell pyroptosis (Fig. 1).

Due to the formation of micropores in the membrane after pyroptosis, cytoplasmic contents are released into extracellular. As shown in Fig. 5e, the LDH release in CDDP + LPAD/GSDME group was significantly increased than others, which further confirmed the largest cell pyroptosis proportion in CDDP + LPAD/GSDME group and was in consistent with the former results (Fig. 5c and d). The Western blot results further proved that GSDME protein level was significantly upregulated by administration of LPAD/GSDME gene delivery system (LPAD/GSDME and CDDP + LPAD/GSDME groups), and the addition of CDDP could induce the cleavage of caspase-3 (Fig. 5f and Fig. S11). The GSDME-N fragments were significantly increased in CDDP + LPAD/GSDME group, which indicated that pyroptosis occurred when cleaved caspase-3 further cleaved enough GSDME protein for GSDME-N fragments (Fig. 5f and Fig. S11).

3.7. LPAD/GSDME gene delivery system combined with CDDP induce ICD response in cells

The aim of simulating pyroptosis was eliciting ICD to initiate the cancer-immunity cycle [14]. When tumor cells undergoing ICD, they tend to produce a series of molecular patterns, such as the exposure calreticulin (CRT) to the cell surface and high mobility group box 1 (HMGB1) secreted by tumor cells to extracellular [12,13]. To confirm the appearance of ICD in the pyroptosis mediated by LPAD/GSDME gene delivery system combined with CDDP, we examined the CRT exposure on the cell surface and the extracellular release of HMGB1 (Fig. 5g and h, Fig. S12). As shown in Fig. 5g and Fig. S12, tumor cells incubated with CDDP or LPAD/GSDME showed almost no CRT expression, while clearly CRT signals were observed in CDDP + LPAD/GSDME group. Meanwhile, compared to controls, HMGB1 were significantly increased in CDDP + LPAD/GSDME group as determined by enzyme-linked immunosorbent assay (ELISA). The results confirmed that the pore-forming gene delivery and chemotherapy synergistic strategy could be applied for inducing strong ICD and activate immune response by pyropotosis pathway.

### 3.8. Accumulation of LPAD-based delivery system

The accumulation of the LPAD vector-based gene delivery system in mice with osteosarcoma was examined by delivering DNA labeled with Cy5 fluorescent molecules (DNA-Cy5). The fluorescence signals in the tumor-bearing mice were monitored at different time points (Fig. 6a and b, and Fig. S13). Compared with the control group, the LPAD/DNA-Cy5 group showed a fluorescence signal in the tumor area at 1 h post injection (Fig. 6a, dotted with red circles). A further increase in the fluorescence signal was recorded at 2 h and kept almost constant till 4 h. At 8 h post injection, the fluorescence signal began to weaken due to natural metabolism.

To further investigate the in vivo accumulation of LPAD/DNA-Cy5 gene delivery system, the mice were sacrificed at 12 h after the administration. The tumor and main organs were collected and visualized, respectively (Fig. 6b and Fig. S13). Compared with the control group and Cy5 group, the tumor in LPAD/DNA-Cy5 group showed a clear fluorescence signal at the 12 h. The fluorescence signals found in liver and kidney were typically attributed to the metabolic pathway of the LPAD/DNA-Cy5 in vivo. In other words, the liver and kidney are the main organs where nanoparticles are eliminated because mesangial cells in the kidney and Kuffer cells and endothelial cells in the liver, in contrast to other organs, are more likely to absorb nanoparticles. And then nanoparticles can be excreted through bile and degraded to achieve elimination.

The high accumulation could be attributed to the suitable particle sizes of LPAD/DNA-Cy5 complexes (Fig. 4b). Moreover, the plentiful hydroxyl groups in LPAD vector can form a hydrating layer, which hinders protein absorption on the complexes and inhibited clearance by the mononuclear phagocyte system (Fig. 4c and d). Therefore, the long circulation and retention time of LPAD/DNA complexes in vivo were obtained, and further benefited the accumulation of the complexes in tumor [38,44]. The results confirmed the potential of the LPAD vector in delivering DNA for gene therapy of osteosarcoma in vivo.

3.9. LPAD/GSDME gene delivery combined with CDDP inhibited osteosarcoma progression in vivo

Owing to the impressive performance of the gene delivery and chemotherapy synergistic strategy in the cellular research, BALB/c mice bearing osteosarcoma were used to investigate its antitumor effects in vivo (Figs. 1, Fig. 6c–h). The administration strategy was shown in Fig. 6c. Tumor growth was recorded by tumor volume measurements taken every two days and eventually all the mice were euthanized and their hearts, livers, spleens, lungs, kidneys, lymph nodes and tumors were collected. After three rounds of different treatments, our results showed that tumors grew rapidly in Control, CDDP and LPAD/GSDME group. In contrast, LPAD/GSDME combined with CDDP treatment effectively inhibited tumor growth (Fig. 6d). Representative images and significantly decrease in tumor weights confirmed the antitumor effect of CDDP + LPAD/GSDME treatment in mice (Fig. 6e and f). The results
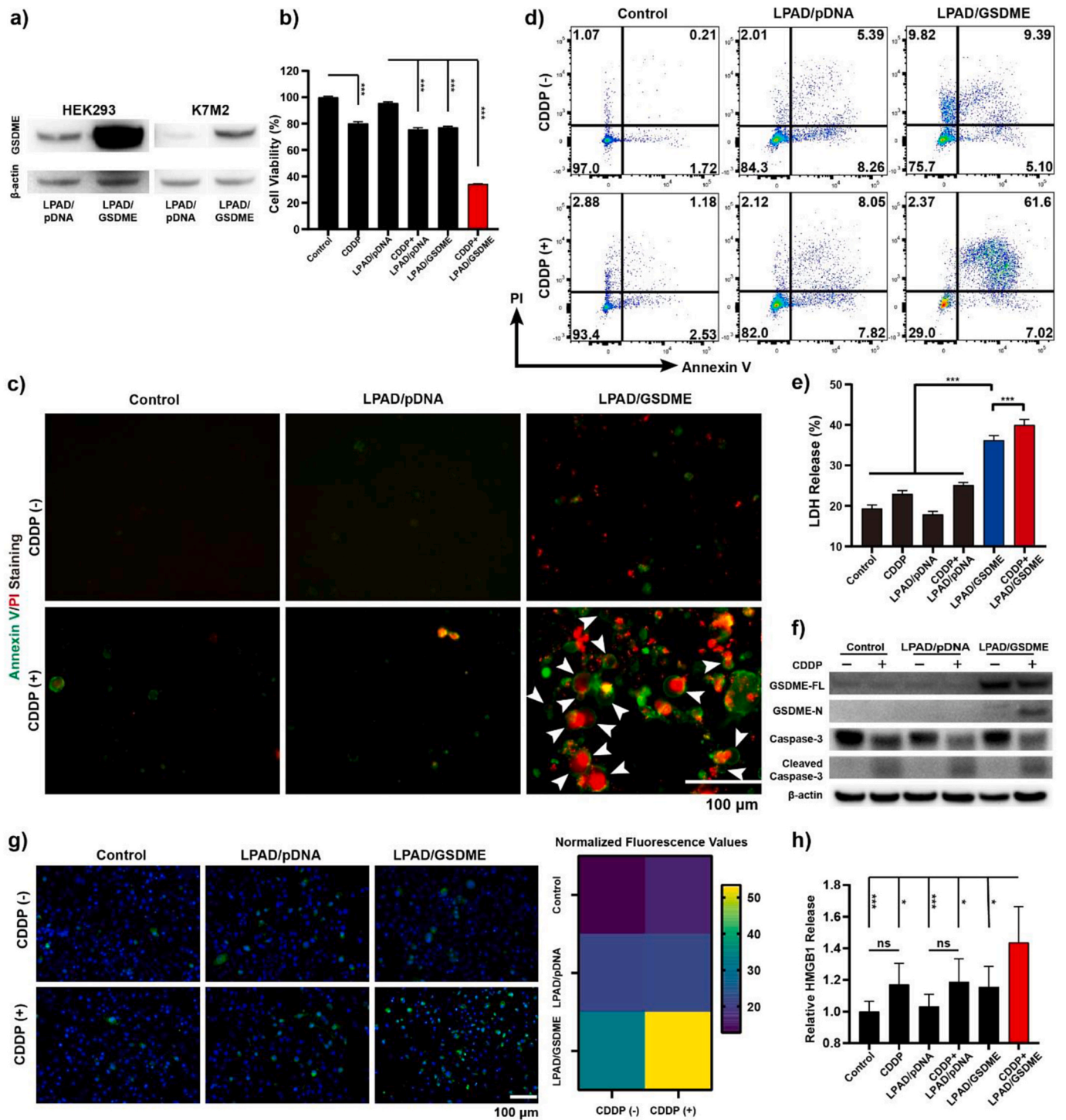
Fig. 5. LPAD/GSDME gene delivery system upregulated GSDME protein levels and successfully induced tumor cell pyroptosis combined with CDDP administration. a) GSDME expressions in HEK293 and K7M2 cell lines treated with LPAD/pDNA or LPAD/GSDME (pDNA was a control plasmid). b) Cell viability of the K7M2 osteosarcoma cell line after various treatments. c) Fluorescence images to confirm the pyroptosis occurrence in K7M2 after different treatments. Annexin V–FITC and PI were added to the cells 15 min before imaging (the morphological changes of pyroptosis were marked with white arrowheads). d) Flow-cytometry measurements to quantify the pyroptosis proportion cells (positive for Annexin V and PI). e) LDH release-based cell death assay in K7M2 cells after different treatments. f) Western blotting detection of full-length GSDME (GSDME-FL), GSDME-N terminal (GSDME-N), pro-caspase-3, and cleaved caspase-3. g) Immuno-fluorescence staining of CRT (Blue, nucleus; Green, CRT). h) HMGB1 secretion. (Control group, cells treated with PBS; CDDP group, cells treated with cisplatin (20 μg/mL); LPAD/pDNA group, cells treated with LPAD/pDNA complexes; CDDP + LPAD/pDNA group, cells treated with LPAD/pDNA complexes and cisplatin (20 μg/mL); LPAD/GSDME group, cells treated with LPAD/GEDME complexes; CDDP + LPAD/GSDME group, cells treated with LPAD/GSDME complexes and cisplatin (20 μg/mL); ns, no significance, *$p < 0.05$, **$p < 0.01$, ***$p < 0.001$.)
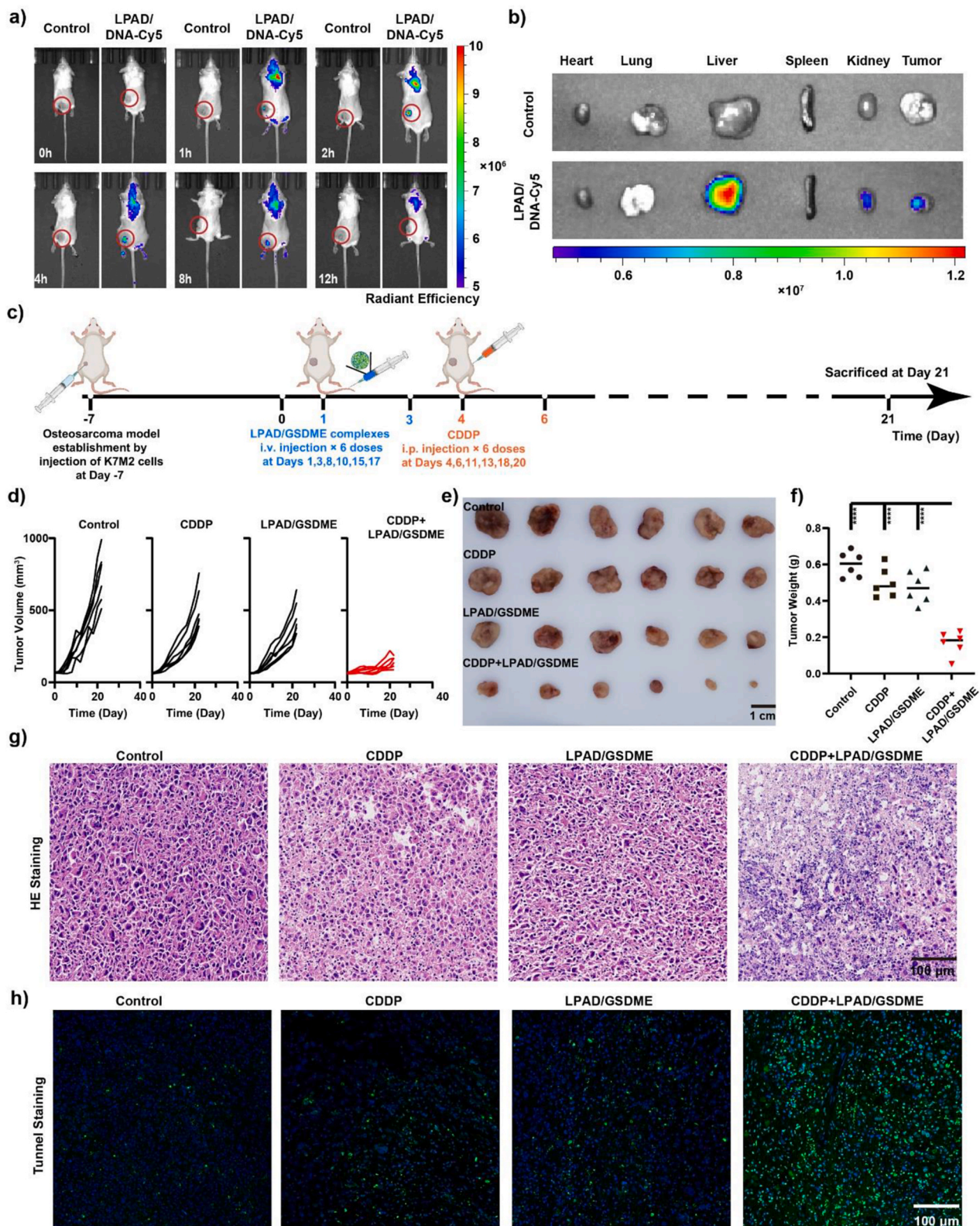
Fig. 6. LPAD vector effectively delivers condensed nucleic acids to K7M2 tumor site and successfully inhibited osteosarcoma progression in vivo, especially combined with CDDP. a) The fluorescent images showed the accumulation of the LPAD/DNA-Cy5 system in osteosarcoma-bearing mice (DNA-Cy5 refer to nucleic acids labeled with Cy5 fluorescent molecule, tumor area in mouse was marked out with red circles). b) Corresponding fluorescent images showed the distribution of LPAD/DNA-Cy5 system in mouse tumor and major organs after 12 h. c) Schematic illustrated the establishment of osteosarcoma model and the treatment strategy of CDDP + LPAD/GSDME. d) Individual growth curves from day 0 to day 21 after different treatments. e,f) Representative tumor images and average tumor weights on day 21 after different treatments. g,h) H&E and tunnel staining images of tumor tissues after different treatments. (Control group, mouse models treated with PBS; CDDP group, mouse models treated with cisplatin (2 μg/g); LPAD/GSDME group, mouse models treated with LPAD/GEDME complexes; CDDP + LPAD/GSDME group, mouse models treated with LPAD/GSDME complexes and cisplatin (2 μg/g); ns, no significance, $*p < 0.05$, $**p < 0.01$, $***p < 0.001$.

suggested that the gene delivery and chemotherapy synergistic strategy might have a strong antitumor effect in vivo.

Representative H&E staining images of osteosarcoma tissues showed that tumor cells in Control, CDDP and LPAD/GSDME groups were relatively regularly arranged, the cytoplasm were plump and the nuclei were intact (Fig. 6g). In the CDDP + LPAD/GSDME group, the tumor cells were sparsely arranged, with severe shrinkage and necrosis, and numerous cell fragments could be observed. Moreover, there are a large number of immune cells in the osteosarcoma tissue of CDDP + LPAD/GSDME group, which indicated that CDDP + LPAD/GSDME combination therapy may reshape the TME of osteosarcoma. Tunnel staining showed a very high positive rate in CDDP + LPAD/GSDME group compared to the other groups, indicating that the CDDP + LPAD/GSDME treatment resulted in a large number of tumor cell deaths (Fig. 6h).

Moreover, H&E staining of major organs, body weight and blood biochemistry of tumor mice were measured to evaluate the biocompatibility and safety of different treatments (Fig. S14). H&E staining of major organs showed no significant pathological changes. While, there were no reduction in mouse body weight during treatment and blood biochemistry assays showed no noticeable difference between the control group and treatment groups. These results suggested that no significant system toxicity or serious side effects were elicited after treatments.

3.10. LPAD/GSDME gene delivery combined with CDDP reshaped the TME of osteosarcoma in vivo

To investigate the antitumor mechanisms underlying the superior antitumor efficacy of the gene delivery and chemotherapy synergistic strategy, we firstly investigated the expression of pyroptosis-related biomarkers (GSDME, Cleaved Caspase-3 and GZMB) (Fig. 7a). The IHC results of tumor tissues showed increased GSDME expression in both the LPAD/GSDME group and CDDP + LPAD/GSDME treatment group, demonstrating the ability of LPAD/GSDME to deliver GSDME gene into osteosarcoma tissues in vivo. In addition, compared with the other treatments, the expression of Cleaved Caspase-3 and GZMB in tumor tissues in CDDP and CDDP + LPAD/GSDME groups also increased. Under the effect of CDDP, caspase-3 existing as inactive proenzyme would undergo proteolytic processing to produce active Cleaved Caspase-3, which can further cleave GSDME to generate GSDME-N terminal domains and finally induce pyroptosis. GZMB is expressed by CTLs and able to induces GSDME-dependent pyroptosis both directly by cleaving GSDME and indirectly by activating caspase-3. Therefore, the IHC results above demonstrated that the combined CDDP + LPAD/GSDME therapy strategy could induce pyroptosis to inhibit osteosarcoma in vivo.

The pore-forming gene delivery combined with chemotherapy strategy was supposed to induce proropotosis-based ICD to reshape the TME of osteosarcoma. Thus, the typical antitumor T lymphocytes were then observed by immunofluorescence (IF) staining (Fig. 7b). It can be observed that CD4$^+$ T cells and CD8$^+$ T cells infiltrating in tumor tissues dramatically increased in CDDP + LPAD/GADME group. The results provided evidences for the TME reshaping in osteosarcoma mediated by CDDP + LPAD/GADME synergistic therapy strategy.

To further analyze the pyroptosis-mediated ICD and TME changes induced by CDDP + LPAD/GSDME treatment, flow cytometry analyses were performed to quantify the changes in immune cell populations (Fig. 8a and b). DCs are associated with the uptake of antigens, which further regulating and maintaining the immune response in vivo (Fig. 1). The maturation of DCs was essential for T cell activation and lead to systemic antitumor immunity. Therefore, CD80$^+$CD86$^+$ mature DCs were quantified in the tumor-draining lymph nodes. The number of mature DCs in the CDDP + LPAD/GSDME group was significantly increased and 2.5 times higher than that in the control group.

And then, the process of mDCs-mediated antitumor immunity was

evaluated by analyzing tumor infiltrating immune related cells, including Th cells, CTLs, M1/M2 macrophages and MDSCs (Fig. 8a and b). In the CDDP + LPAD/GSDME group, the numbers of CD3$^+$CD4$^+$ T cells (Ths) and CD3$^+$CD8$^+$ T cells (CTLs) in osteosarcoma were also significantly higher. To be more specify, CD3$^+$CD4$^+$ T cells and CD3$^+$CD8$^+$ T cells in CDDP + LPAD/GSDME group were 3.4-fold and 2.7-fold of control group, respectively. In other words, the CDDP + LPAD/GSDM treatment successfully recruited more antitumor immune cells. In addition, M1-like macrophages which were associated with immune activation in tumors increased markedly in the CDDP + LPAD/GSDME group; Typical immune cells associated with immune suppression in tumors including M2-like macrophages and MDSCs were significantly downregulated by CDDP + LPAD/GSDME treatment. Therefore, it can be concluded that the gene delivery and chemotherapy synergistic strategy could reshape the TME to "hot" with recruiting more antitumor immune cells and increase immune activated M1-macrophages, and decrease immune suppressive immune cells.

Inflammatory cytokines are important components in TME. In this study, the changes of the secretion of inflammatory cytokines in the TME of osteosarcoma were detected by ELISA (Fig. 8c and Fig. S15). Chemokine (*C*-X-C motif) ligand 10 (CXCL10), which is related to CD8$^+$ T cells recruitment, showed an increased expression in the CDDP + LPAD/GSDME group. The result further clarified the increased CD3$^+$CD4$^+$ T cells and CD3$^+$CD8$^+$ T cells in TME in CDDP + LPAD/GSDME group (Fig. 8a and b). Some interleukin factors can also help generate an immune activated "hot" TME. IL-2 and IL-12 can promote T cells and NK cells to produce IFN-γ and TNF-α, thus increasing the antitumor activity of NK cells and T cells. Our results showed that CDDP + LPAD/GSDME treatment can significantly stimulate the secretion of these two cytokines in the TME of osteosarcoma. While IFN-γ and TNF-α, which are directly related to TME activation and antitumor efficiency, showed highest expression in CDDP + LPAD/GSDME group. Cytokines can not only promote immune system activation but also suppress it. IL-4 and IL-10 are two interleukin factors that contribute to the immune response suppression, and their secretion were significantly inhibited after CDDP + LPAD/GSDME therapy. Thus, the study of inflammatory cytokines secretion further confirmed that the changes in TME caused by CDDP + LPAD/GSDME treatment was beneficial for tumor inhibition.

3.11. Systemic antitumor immune response

Studies have proved that powerful immune stimulation by pyroptosis-based ICD could realize systemic antitumor immune response and inhibit the growth of distant tumors [37,44]. The establishment of tumor models was carried out as shown in Fig. 8d. The osteosarcoma cells were firstly injected into the left back of mice to produce the primary tumor. Then the right back of mice was subcutaneously inoculated with the same amount tumor cells as the distant tumor as shown in Fig. 8d after different treatments. Distant tumor volume changes were recorded, and all tumors were collected and imaged at the end (Fig. 8e–g). As shown in Fig. 8e, no distant tumors were detected in CDDP + LPAD/GSDME group, while distant tumor occurrence in control group was 5/7. Moreover, the growth curves in Fig. 8f further proved the inhibition of distant tumors in CDDP + LPAD/GSDME group. The results may be attributed to the increased IL-2, IL-12, IFN-γ and TNF-α secretions (Fig. 8c and Fig. S15), which can offer the body enhanced systemic immune response. Furthermore, CDDP + LPAD/GSDME treatment has effectively inhibited the growth of the primary tumor at the initial stage, which was consistent with what we observed in Fig. 6c. But it gradually returned to its normal rate following the termination of administrations (Fig. 8g). The rechallenge experiment results further demonstrated that the pore-forming GSDME gene delivery together with CDDP administration can arouse the strongest systemic antitumor immune response, and leading the most effective distant tumors suppression. But this curative effect needs adequate courses of treatment for successful primary tumor suppression.
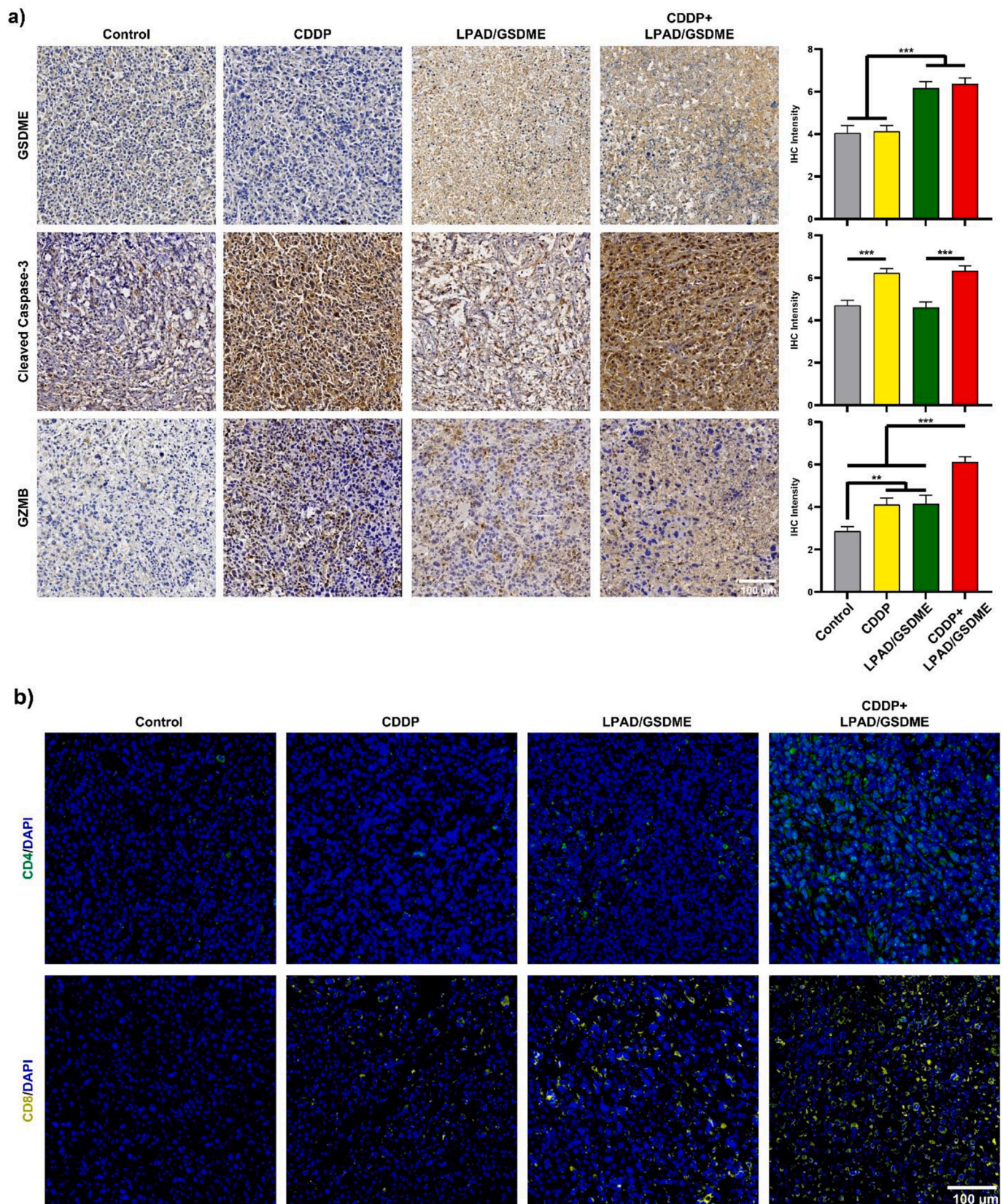
Fig. 7. IHC staining IHC and IFstaining to investigate pyroptosis mechanism and immune infiltration with different treatments. a) Representative images and corresponding quantifications of IHC for detecting GSDME, cleaved Caspase-3 and GZMB expressions in tumor tissues after different treatments. b) IF staining for CD4$^+$ T cells and CD8$^+$ T cells infiltrating in tumor tissues after various treatments. (Control group, mouse models treated with PBS; CDDP group, mouse models treated with cisplatin (2 μg/g); LPAD/GSDME group, mouse models treated with LPAD/GEDME complexes; CDDP + LPAD/GSDME group, mouse models treated with LPAD/GSDME complexes and cisplatin (2 μg/g)).
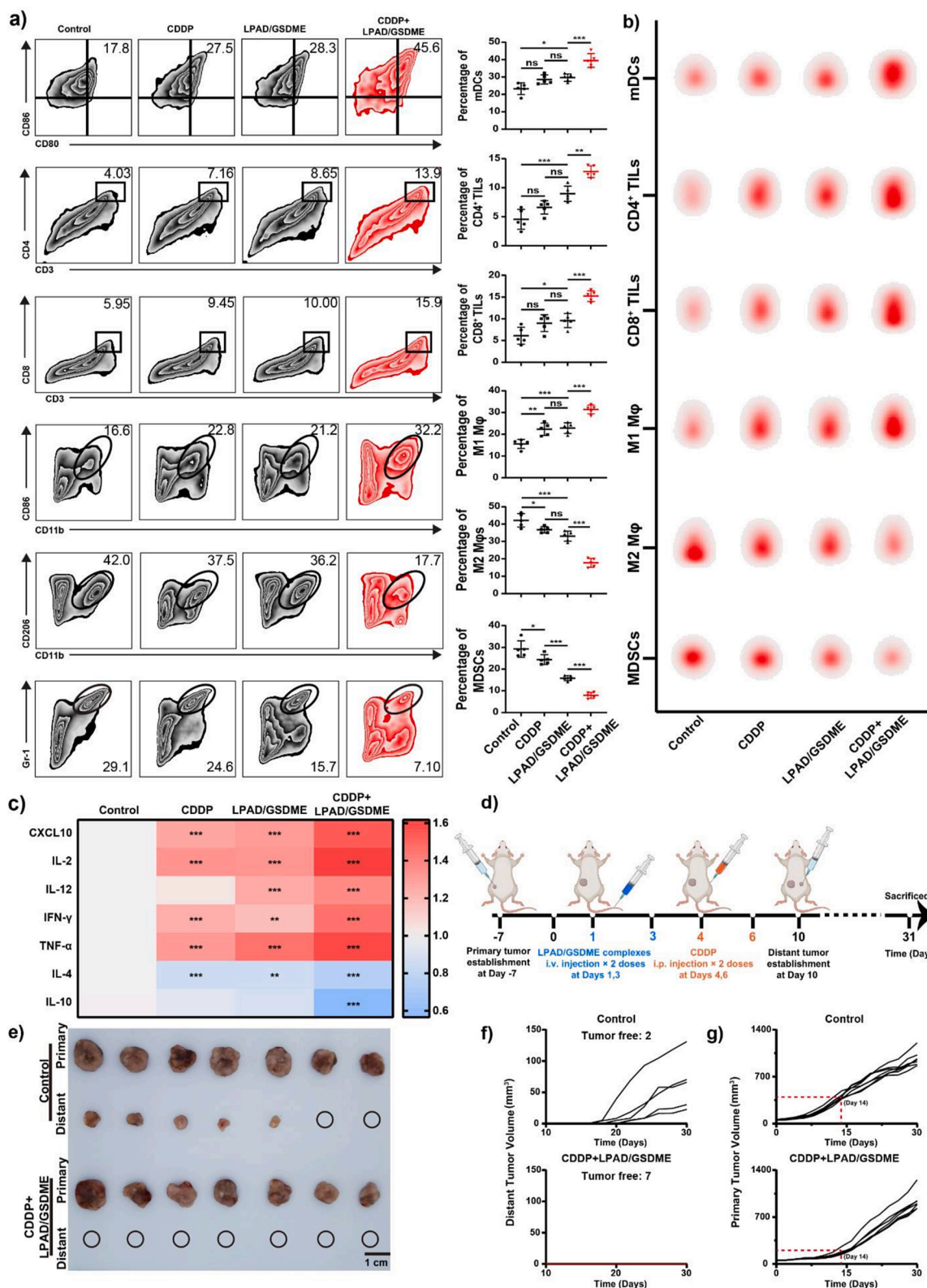
Fig. 8. Administrations of LPAD/GSDME and CDDP triggers pyroptosis for turning "cold" osteosarcoma into "hot" and eliciting antitumor immunity. a) Flow cytometric quantify the percentage of matured DCs (mDCs) isolated from lymph nodes (CD11c$^+$CD80$^+$CD86$^+$), and Ths in TILs (CD3$^+$CD4$^+$), CTLs in tumor-infiltrating-lymphocytes (CD3$^+$CD8$^+$), M1-macrophages (M1 Mφ) (CD11b$^+$CD86$^+$), M2-macrophages (M2 Mφ) (CD11b$^+$CD206$^+$) and MDSCs (CD11b$^+$Gr-1$^+$) isolated from tumor tissues. b) Corresponding concatenation analysis. c) Heat map of relatively concentrations of cytokines in tumor tissues measured by ELISA. d) Schematic illustrated the treatment strategy of CDDP + LPAD/GSDME against primary and distant tumors in rechallenge osteosarcoma mouse models. e) Representative images, f) distant and g) primary tumor volume changes in the rechallenge osteosarcoma mouse models. (Control group, mouse models treated with PBS; CDDP group, mouse models treated with cisplatin (2 μg/g); LPAD/GSDME group, mouse models treated with LPAD/GEDME complexes; CDDP + LPAD/GSDME group, mouse models treated with LPAD/GSDME complexes and cisplatin (2 μg/g); ns, no significance, *$p < 0.05$, **$p < 0.01$, ***$p < 0.001$.)

4. Discussion

Osteosarcoma is one of the top five leading cause of cancer death in adolescent [1,2]. The efficient of traditional treatments is limited while metastasis or recurrence happened in patients. Moreover, the average 5-year event-free survival of patients with osteosarcoma has not been improved significantly in the last few decades. The occurrence and development of cancer is the result of immunological imbalance [47–49]. Immunotherapy focus on restoring and maintaining the immune system ability for monitoring and eliminating cancers, which provides a promising strategy for osteosarcoma. The immune checkpoint blocking therapy and chemotherapy-immunotherapy provided some improvements for osteosarcoma treatment. However, the low patient response, poor drug specificity and limited pyroptosis induction ability make the treatments unable to achieve the desired endings [4–6].

GSDMs is the key executor of pyroptosis, and GSDME is proved to suppress tumor growth by activating antitumor immunity [14,15,18]. Thus, we firstly investigated the expression and prognosis of GSDMs and their relationships with immune infiltration in osteosarcoma by using bioinformatics analysis (Fig. 2, Fig. S1). Three gasdermin family members, GSDMA, GSDMB, and GSDME, were closely associated with the overall survival of osteosarcoma patients (Fig. 2a). GO and KEGG analyses proved that GSDMs-associated genes were mainly involved in secretion of IL-1 and IL-18, the formation of inflammasome, and the participation in apoptosis process (Fig. 2b). The results indicated that gasdermin family is mainly related to tumor suppression and inflammation. ESTIMATE analysis further confirmed that GSDMA, GSDMD and GSDME were positively linked to the abundance of immune cells and stromal cells in osteosarcoma, and GSDMD and GSDME were shown to be favorably correlated with up to 27 different types of immune cells (Fig. 2c and d). Taken the above bioinformatics analysis results together, we can conclude that GSDME is closely associated with prognosis and immune infiltration in TME of osteosarcoma patients.

Multiplex immunohistochemical of immune cell infiltration in clinical samples confirmed the immune suppressive TME of osteosarcoma (Fig. 3a). Then qRT-PCR were performed to evaluate GSDMs expressions in both osteosarcoma cell lines and clinical samples (Fig. 3b and c). The GSDME expression in tumor tissue microassay further confirmed the potential of GSDME as a target for effective osteosarcoma inhibition (Fig. 3d–f), and pyroptosis-mediated TME reshape of osteosarcoma was proposed and investigated by GSDME gene delivery.

LPAD polycation was prepared for delivering pore-forming GSDME protein encoding functional plasmid to upregulate GEDME protein level in osteosarcoma (Figs. 4 and 5a). The LPAD vectors showed great potential in condensing and delivering DNA with suitable sizes and potentials (Fig. 4a and b). Atomistic molecular dynamics simulations proved that the abundant hydroxyl groups in LPAD polycations provided more impressive water molecule associations than PEI by enhancing coulombic interaction (Fig. 4c and Fig. S5), which means a stronger hydration ability and benefits to prevent potential cytotoxicity caused by the positive charge, as well as hinders protein absorption on the complexes (Fig. 4d and e) and inhibited clearance by the mononuclear phagocyte system in vivo [37,44]. Therefore, the LPAD vectors shows good biocompatibility, and long retention time and high accumulation in tumor in vivo (Fig. 4e and f, Fig. 6a and b, Fig. S6 and Fig. S8).

The combination of gene delivery and chemotherapy successfully induced pyroptosis and stimulated ICD, which provided an impressive osteosarcoma inhibition (Figs. 5 and 6). LPAD/GSDME gene delivery system upregulated GSDME proteins in osteosarcoma, followed administration of cisplatin therapeutic chemical activated caspase-3 and cleaved GSDME proteins (Fig. 5f and Fig. S11). The GSDME-N fragments assemble and translocated to cell membrane to inducing propotosis. CRT and HMGB1 release further confirmed the occurrence of ICD (Fig. 5g and h). Series of results in vivo showed exciting tumor inhibition and TME reshaping ability to immune activation direction (Figs. 6–8), which proved the potential of pore-forming gene delivery for osteosarcoma

therapy together with chemical administration.

Studies have proved that powerful immune stimulation could realize systemic antitumor immune response and inhibit the growth of distant tumors [33,40]. Rechallenge experiment was carried out and exciting distant tumor inhibition were observed (Fig. 8d–f). The results may be attributed to the increased IL-2, IL-12, IFN-γ and TNF-α secretions (Fig. 8c and Fig. S15), which can offer the body enhanced systemic immune response. The rechallenge experiment results demonstrated that the GSDME gene delivery together with CDDP administration can arouse the strongest systemic antitumor immune response, which is of great significance to solve the intractable recurrence and metastasis.

Owing to the low incidence of osteosarcoma, additional research and a larger sample size are still required. Our research has demonstrated that pore-forming gene delivery is currently a viable treatment option for osteosarcoma. It is therefore necessary to investigate and optimize existing cationic gene delivery platforms further with larger animal experiments, which is possible due to our platform's scalability.

5. Conclusion

Overall, we found the GSDME in gasdermin family was positively correlated with prognosis and immune infiltration of osteosarcoma patients. Low-toxic cationic vector LPAD with high hydration ability was then prepared to deliver the pore-forming protein encoding genes to upregulate GSDME protein level in osteosarcoma for efficient TME reshaping via enhanced pyroptosis induction. The following administration of cisplatin therapeutic chemical successfully started the pyroptosis process. The pyroptosis-mediated synergistic gene delivery and chemotherapy provide impressive tumor inhibition and TME reshaping ability to immune activation direction. The strategy also can arouse systemic antitumor immune response and inhibited the growth of distant tumors. Moreover, the CDDP + LPAD/GSDME possesses good blood compatibility and did not cause toxicity to organs. Such a pyroptosis-dependent pore-forming gene delivery and chemical administration strategy not only contribute to the inhibition of osteosarcoma, but also provided potential solution for osteosarcoma recurrence and metastasis. Due to the importance of gasdermin proteins in pyrotosis, the study also contributes valuable information for tumors with high immune suppressive TME.

Ethics approval and consent to participate

Osteosarcoma tissues punctured from patients were obtained and histologically confirmed by Beijing Jishuitan Hospital. We have also obtained the informed consent for this experiment with human subjects. The privacy rights of human subjects were respected throughout the process. This study was approved by the ethics committee of Beijing Jishuitan Hospital (202002–07). All animal studies were approved by Animal Ethics Committee of the Beijing Jishuitan Hospital.

CRediT authorship contribution statement

Jing-Jun Nie: Writing – original draft, Project administration, Funding acquisition, Conceptualization. **Bowen Zhang:** Writing – original draft, Investigation. **Peng Luo:** Writing – original draft, Investigation. **Maoguo Luo:** Investigation, Formal analysis. **Yuwen Luo:** Visualization, Formal analysis. **Jingjing Cao:** Investigation, Formal analysis. **Honggang Wang:** Validation, Data curation. **Jianping Mao:** Project administration, Data curation. **Yonggang Xing:** Validation, Investigation. **Weifeng Liu:** Resources, Data curation. **Yuning Cheng:** Methodology, Formal analysis. **Renxian Wang:** Validation, Resources. **Yajun Liu:** Writing – review & editing, Supervision. **Xinbao Wu:** Project administration, Funding acquisition, Data curation. **Xieyuan Jiang:** Supervision, Data curation. **Xiaoguang Cheng:** Writing – review & editing, Project administration. **Chi Zhang:** Project administration, Formal analysis. **Da-Fu Chen:** Writing – review & editing, Funding

acquisition, Conceptualization.

Declaration of competing interest

Da-Fu Chen is an editorial board member for *Bioactive Materials* and was not involved in the editorial review or the decision to publish this article. All authors declare that there are no competing interests.

Acknowledgements

Appendix A. Supplementary data

Supplementary data to this article can be found online at https://doi.org/10.1016/j.bioactmat.2024.05.009.

References

[1] H.C. Beird, S.S. Bielack, A.M. Flanagan, J. Gill, D. Heymann, K.A. Janeway, J. A. Livingston, R.D. Roberts, S.J. Strauss, R. Gorlick, Osteosarcoma, Nat. Rev. Dis. Prim. 8 (2022) 77.

[2] H. Tian, J. Cao, B. Li, E.C. Nice, H. Mao, Y. Zhang, C. Huang, Managing the immune microenvironment of osteosarcoma: the outlook for osteosarcoma treatment, Bone Res. 11 (2023) 11.

[3] J.A. Marin-Acevedo, E.O. Kimbrough, Y. Lou, Next generation of immune checkpoint inhibitors and beyond, J. Hematol. Oncol. 14 (2021) 45.

[4] H.A. Tawbi, M. Burgess, V. Bolejack, B.A. Van Tine, S.M. Schuetze, J. Hu, S. D'Angelo, S. Attia, R.F. Riedel, D.A. Priebat, S. Movva, L.E. Davis, S.H. Okuno, D. R. Reed, J. Crowley, L.H. Butterfield, R. Salazar, J. Rodriguez-Canales, A.J. Lazar, I. I. Wistuba, L.H. Baker, R.G. Maki, D. Reinke, S. Patel, Pembrolizumab in advanced soft-tissue sarcoma and bone sarcoma (SARC028): a multicentre, two-cohort, single-arm, open-label, phase 2 trial, Lancet Oncol. 18 (2017) 1493–1501.

[5] T. Zhu, J. Han, L. Yang, Z. Cai, W. Sun, Y. Hua, J. Xu, Immune microenvironment in osteosarcoma: components, therapeutic strategies and clinical applications, Front. Immunol. 13 (2022) 907550.

[6] J. Gill, R. Gorlick, Advancing therapy for osteosarcoma, Nat. Rev. Clin. Oncol. 18 (2021) 609–624.

[7] M.A. Anwar, C. El-Baba, M.H. Elnaggar, Y.O. Elkholy, M. Mottawea, D. Johar, T. S. Al Shehabi, F. Kobeissy, C. Moussalem, E. Massaad, I. Omeis, N. Darwiche, A. H. Eid, Novel therapeutic strategies for spinal osteosarcomas, Semin. Cancer Biol. 64 (2020) 83–92.

[8] P.S. Meltzer, L.J. Helman, New horizons in the treatment of osteosarcoma, N. Engl. J. Med. 385 (2021) 2066–2076.

[9] G. Kroemer, C. Galassi, L. Zitvogel, L. Galluzzi, Immunogenic cell stress and death, Nat. Immunol. 23 (2022) 487–500.

[10] W. Gao, X. Wang, Y. Zhou, X. Wang, Y. Yu, Autophagy, ferroptosis, pyroptosis, and necroptosis in tumor immunotherapy, Signal Transduct. Targeted Ther. 7 (2022) 196.

[11] G. Kroemer, L. Galluzzi, O. Kepp, L. Zitvogel, Immunogenic cell death in cancer therapy, Annu. Rev. Immunol. 31 (2013) 51–72.

[12] D.V. Krysko, A.D. Garg, A. Kaczmarek, O. Krysko, P. Agostinis, P. Vandenabeele, Immunogenic cell death and DAMPs in cancer therapy, Nat. Rev. Cancer 12 (2012) 860–875.

[13] M. Obeid, A. Tesniere, F. Ghiringhelli, G.M. Fimia, L. Apetoh, J.L. Perfettini, M. Castedo, G. Mignot, T. Panaretakis, N. Casares, D. Métivier, N. Larochette, P. van Endert, F. Ciccosanti, M. Piacentini, L. Zitvogel, G. Kroemer, Calreticulin exposure dictates the immunogenicity of cancer cell death, Nat. Med. 13 (2007) 54–61.

[14] Q. Wang, Y. Wang, J. Ding, C. Wang, X. Zhou, W. Gao, H. Huang, F. Shao, Z. Liu, A bioorthogonal system reveals antitumour immune function of pyroptosis, Nature 579 (2020) 421–426.

[15] G. Privitera, N. Rana, A. Armuzzi, T.T. Pizarro, The gasdermin protein family: emerging roles in gastrointestinal health and disease, Nat. Rev. Gastroenterol. Hepatol. 20 (2023) 366–387.

[16] W. Deng, Y. Bai, F. Deng, Y. Pan, S. Mei, Z. Zheng, R. Min, Z. Wu, W. Li, R. Miao, Z. Zhang, T.S. Kupper, J. Lieberman, X. Liu, Streptococcal pyrogenic exotoxin B cleaves GSDMA and triggers pyroptosis, Nature 602 (2022) 496–502.

[17] Z. Zhou, H. He, K. Wang, X. Shi, Y. Wang, Y. Su, Y. Wang, D. Li, W. Liu, Y. Zhang, L. Shen, W. Han, L. Shen, J. Ding, F. Shao, Granzyme A from cytotoxic lymphocytes cleaves GSDMB to trigger pyroptosis in target cells, Science 368 (2020) eaaz7548.

[18] Z. Zhang, Y. Zhang, S. Xia, Q. Kong, S. Li, X. Liu, C. Junqueira, K.F. Meza-Sosa, T.M. Y. Mok, J. Ansara, S. Sengupta, Y. Yao, H. Wu, J. Lieberman, Gasdermin E suppresses tumour growth by activating anti-tumour immunity, Nature 579 (2020) 415–420.

[19] Y. Wang, W. Gao, X. Shi, J. Ding, W. Liu, H. He, K. Wang, F. Shao, Chemotherapy drugs induce pyroptosis through caspase-3 cleavage of a gasdermin, Nature 547 (2017) 99–103.

[20] Y. Xiao, T. Zhang, X. Ma, Q.-C. Yang, L.-L. Yang, S.-C. Yang, M. Liang, Z. Xu, Z.- J. Sun, Microenvironment-responsive prodrug-induced pyroptosis boosts cancer immunotherapy, Adv. Sci. 8 (2021) 2101840.

[21] J. Zhang, B. Zhou, R. Sun, Y. Ai, K. Cheng, F. Li, B. Wang, F. Liu, Z. Jiang, W. Wang, D. Zhou, H. Chen, Q. Wu, The metabolite α-KG induces GSDMC-dependent pyroptosis through death receptor 6-activated caspase-8, Cell Res. 31 (2021) 980–997.

[22] X. Fang, Z. Chen, W. Zhou, T. Li, M. Wang, Y. Gao, S. Ma, Y. Feng, S. Du, P. Lan, H. Chen, J. Wei, S. Zhang, Z. Li, X. Liu, H. Zhang, X. Guo, J. Luo, Boosting glioblastoma therapy with targeted pyroptosis induction, Small 19 (2023) 2207604.

[23] X. Song, H. Huang, L. Xia, W. Jia, S. Yang, C. Wang, Y. Chen, Engineering 2D multienzyme-mimicking pyroptosis inducers for ultrasound-augmented catalytic tumor nanotherapy, Adv. Sci. 10 (2023) 2301279.

[24] Y. Bao, Y. Ge, M. Wu, Z. Mao, J. Ye, W. Tong, Record-high ultrasound-sensitive NO nanogenerators for cascade tumor pyroptosis and immunotherapy, Adv. Sci. 10 (2023) 2302278.

[25] G. Xing, X. Yu, Y. Zhang, S. Sheng, L. Jin, D. Zhu, L. Mei, X. Dong, F. Lv, Macrophages-based biohybrid microrobots for breast cancer photothermal immunotherapy by inducing pyroptosis, Small 20 (2023) 202305526.

[26] M. Chen, H. Liao, Z. Bu, D. Wang, C. Fang, X. Liang, H. Li, J. Liu, K. Zhang, D. Su, Pyroptosis activation by photodynamic-boosted nanocatalytic medicine favors malignancy recession, Chem. Eng. J. 441 (2022) 136030.

[27] Z. Zhou, R. Yang, J. Dong, Y. Di, Y. Yang, Y. Huang, X. Yang, W. Liu, J. Wang, P. Liu, Z. Gu, M. Sun, Pore forming-mediated intracellular protein delivery for enhanced cancer immunotherapy, Sci. Adv. 8 (2022) eabq4659.

[28] Y. Tang, H.K. Bisoyi, X.-M. Chen, Z. Liu, X. Chen, S. Zhang, Q. Li, Pyroptosis- mediated synergistic photodynamic and photothermal immunotherapy enabled by a tumor-membrane-targeted photosensitive dimer, Adv. Mater. 35 (2023) 2300232.

[29] J.A. Kulkarni, D. Witzigmann, S.B. Thomson, S. Chen, B.R. Leavitt, P.R. Cullis, R. van der Meel, The current landscape of nucleic acid therapeutics, Nat. Nanotechnol. 16 (2021) 630–643.

[30] H.J. Vaughan, J.J. Green, S.Y. Tzeng, Cancer-targeting nanoparticles for combinatorial nucleic acid delivery, Adv. Mater. 32 (2020) 1901081.

[31] K. Li, J. Guo, Y. Ming, S. Chen, T. Zhang, H. Ma, X. Fu, J. Wang, W. Liu, Y. Peng, A circular RNA activated by TGFβ promotes tumor metastasis through enhancing IGF2BP3-mediated PDPN mRNA stability, Nat. Commun. 14 (2023) 6876.

[32] S. Yang, Y. Wu, W. Zhong, R. Chen, M. Wang, M. Chen, GSH/pH dual activatable cross-linked and fluorinated PEI for cancer gene therapy through endogenous iron de-hijacking and in situ ROS amplification, Adv. Mater. 36 (2023) 2304098.

[33] H. Jiang, H. Fu, T. Min, P. Hu, J. Shi, Magnetic-manipulated NK cell proliferation and activation enhance immunotherapy of orthotopic liver cancer, J. Am. Chem. Soc. 145 (2023) 13147–13160.

[34] B. Lee, K. Gries, A.R. Valimukhametova, R.L. McKinney, R. Gonzalez-Rodriguez, U. C. Topkiran, J. Coffer, G.R. Akkaraju, A.V. Naumov, In vitro prostate cancer treatment via CRISPR-Cas9 gene editing facilitated by polyethyleneimine-derived graphene quantum dots, Adv. Funct. Mater. 33 (2023) 2305506.

[35] Y. Hu, L. Lin, J. Chen, A. Maruyama, H. Tian, X. Chen, Synergistic tumor immunological strategy by combining tumor nanovaccine with gene-mediated extracellular matrix scavenger, Biomaterials 252 (2020) 120114.

[36] R. Xu, L. Huang, J. Liu, Y. Zhang, Y. Xu, R. Li, S. Su, X. Xu, Remodeling of mitochondrial metabolism by a mitochondria-targeted RNAi nanoplatform for effective cancer therapy, Small 20 (2023) 202305923.

[37] X. Zhao, K. Guo, K. Zhang, S. Duan, M. Chen, N. Zhao, F.-J. Xu, Orchestrated yolk-shell nanohybrids regulate macrophage polarization and dendritic cell maturation for oncotherapy with augmented antitumor immunity, Adv. Mater. 34 (2022) 2108263.

[38] D. Yu, Y. Wang, S. Qu, N. Zhang, K. Nie, J. Wang, Y. Huang, D. Sui, B. Yu, M. Qin, F.-J. Xu, Controllable star cationic poly(disulfide)s achieve genetically cascade catalytic therapy by delivering bifunctional fusion plasmids, Adv. Mater. 35 (2023) 2108263.

[39] F.-J. Xu, Versatile types of hydroxyl-rich polycationic systems via O-heterocyclic ring-opening reactions: from strategic design to nucleic acid delivery applications, Prog. Polym. Sci. 78 (2018) 56–91.

[40] J.-J. Nie, Y. Liu, Y. Qi, N. Zhang, B. Yu, D.-F. Chen, M. Yang, F.-J. Xu, Charge-reversal nanocomolexes-based CRISPR/Cas9 delivery system for loss-of-function oncogene editing in hepatocellular carcinoma, J. Contr. Release 333 (2021) 362–373.

[41] N. Zhao, L. Yan, X. Zhao, X. Chen, A. Li, D. Zheng, X. Zhou, X. Dai, F.-J. Xu, Versatile types of organic/inorganic nanohybrids: from strategic design to biomedical applications, Chem. Rev. 119 (2019) 1666–1762.

[42] L. Zheng, Y. Zhu, Y. Sun, S. Xia, S. Duan, B. Yu, J. Li, F.-J. Xu, Flexible modulation of cellular activities with cationic photosensitizers: insights of alkyl chain length on reactive oxygen species antimicrobial mechanisms, Adv. Mater. 35 (2023) 2302943.

[43] E. Blanco, H. Shen, M. Ferrari, Principles of nanoparticle design for overcoming biological barriers to drug delivery, Nat. Biotechnol. 33 (2015) 941.

[44] T. Wu, Y. Dai, Tumor microenvironment and therapeutic response, Cancer Lett. 387 (2017) 61–68.

[45] A. Alfranca, L. Martinez-Cruzado, J. Tornin, A. Abarrategi, T. Amaral, E. de Alava, P. Menendez, J. Garcia-Castro, R. Rodriguez, Bone microenvironment signals in osteosarcoma development, Cell. Mol. Life Sci. 72 (2015) 3097–3113.

[46] D.-F. Chen, B.W. Zhang, J. Cao, H. Wang, P. Luo, W. Liu, X. Niu, R. Wang, J.-J. Nie, Preparation of polycation with hydroxyls for enhanced delivery of miRNA in osteosarcoma therapy, Biomater. Sci. 10 (2022) 2844–2856.

[47] P.D. Sadowitz, B.A. Hubbard, J.C. Dabrowiak, J. Goodisman, K.A. Tacka, M. K. Aktas, M.J. Cunningham, R.L. Dubowy, A.K. Souid, Kinetics of cisplatin binding to cellular DNA and modulations by thiol-blocking agents and thiol drugs, Drug Metab. Dispos. 30 (2002) 183–190.

[48] D.M. Altmann, A nobel prize-worthy pursuit: cancer immunology and harnessing immunity to tumour neoantigens, Immunology 155 (2018) 283–284.

[49] D. Hanahan, R.A. Weinberg, Hallmarks of cancer: the next generation, Cell 144 (2011) 646–674.